Journal of Chromatography A 1677 (2022) 463308

Contents lists available at ScienceDirect

Journal of Chromatography A

journal homepage: www.elsevier.com/locate/chroma

High-performance thin-layer chromatography – antibacterial assay first reveals bioactive clerodane diterpenes in giant goldenrod (*Solidago gigantea* Ait.)

Márton Baglyas[a], Péter G. Ott[a], Zsófia Garádi[b], Vesna Glavnik[c], Szabolcs Béni[b], Irena Vovk[c], Ágnes M. Móricz[a,*]

[a] Centre for Agricultural Research, ELKH, Plant Protection Institute, Herman O. Str. 15, Budapest 1022, Hungary
[b] Department of Pharmacognosy, Faculty of Pharmaceutical Sciences, Semmelweis University, Üllői Str. 26, Budapest 1085, Hungary
[c] Laboratory for Food Chemistry, National Institute of Chemistry, Hajdrihova 19, Ljubljana SI-1000, Slovenia

ARTICLE INFO

Article history:
Received 15 May 2022
Revised 4 July 2022
Accepted 5 July 2022
Available online 9 July 2022

Keywords:
High-performance thin-layer chromatography – effect-directed analysis
High-performance thin-layer chromatography – MS^n
HPTLC – *Rhodococcus fascians*
Giant goldenrod (*Solidago gigantea* Ait.)
Antibacterial clerodane diterpenes

ABSTRACT

The present work introduces a high-performance thin-layer chromatography (HPTLC)–direct bioautography method using the Gram-positive plant pathogenic bacterium, *Rhodococcus fascians*. The screening and isolation procedure comprised of a non-targeted high-performance thin-layer chromatography-effect-directed analysis (HPTLC–EDA) against *Bacillus subtilis, B. subtilis* subsp. *spizizenii, R. fascians*, and *Aliivibrio fischeri*, a targeted HPTLC–mass spectrometry (MS), and bioassay-guided column chromatographic (preparative flash and semi-preparative HPLC) fractionation and purification. The developed new separation methods enabled the discovery of four bioactive *cis*-clerodane diterpenes, solidagoic acid H (**1**), solidagoic acid E (**2**), solidagoic acid I (**3**), and solidagoic acid F (**4**), in the *n*-hexane extract of giant goldenrod (*Solidago gigantea* Ait.) leaf for the first time. These compounds were identified by 1D and 2D nuclear magnetic resonance (NMR) spectroscopy. The initially used HPTLC method (chloroform – ethyl acetate – methanol 15:3:2, *V/V/V*) was changed (to *n*-hexane – isopropyl acetate – methanol – acetic acid 29:20:1:1, *V/V/V/V*) to achieve the separation of the closely related isomer pairs (**1**–**2** and **3**–**4**). Compounds **1** and **3** exhibited moderate antibacterial activity against the Gram-positive *B. subtilis* subsp. *spizizenii* and *R. fascians* bacterial strains in microdilution assays with half-maximal inhibitory concentration (IC_{50}) values in the range of 32.3–64.4 µg/mL. The mass spectrometric fragmentation of the isolated compounds was interpreted and their previously published NMR assignments lacking certain resonances were completed.

1. Introduction

Traditional healthcare recognized the therapeutical importance of plant-derived drugs since ancient times, and among others plant extracts, decoctions, and essential oils are applied for the treatment of various diseases. However, in modern medicine the elimination of the interfering molecules and the use of one- or two-compound based medicines are preferred. Thus, there is an increasingly growing demand for the isolation and determination of effective compounds with inexhaustible structural and functional diversity from bioactive natural sources [1,2].

Solidago gigantea Ait. (giant goldenrod) originated from North America and is considered as a quite successful, threatening, highly invasive weed species in most of Europe [3]. Because of its beneficial pharmacological effects (diuretic, antiphlogistic, antioxidant, antispasmodic) [4], it is also recognized as a medicinal plant. The dried giant goldenrod's leafy, and/or flowering aerial parts are used in phytotherapy (*Solidaginis herba*) [5]. Giant goldenrod contains a wide variety of secondary metabolites, *e.g.* flavonoids [6], phenolic acids [7], and monoterpenoids [8], sesquiterpenoids [9], diterpenoids [10,11] as well as triterpenoids [12]. The antibacterial activity of roots and aboveground parts of various goldenrods has been demonstrated several times [13–15]. Acetylenes (matricaria and dehydromatricaria esters) [16], clerodane diterpenes (*e.g.* kingidiol and solidagoic acid A) [10], labdane diterpenes (solidagenone and presolidagenones) [17], benzyl benzoate derivative [16], and essential oil terpenes [18] have been established as antibacterial components of goldenrod roots, while the pharmacolog-

* Corresponding author.
E-mail address: moricz.agnes@atk.hu (Á.M. Móricz).

https://doi.org/10.1016/j.chroma.2022.463308

ical effect of the aboveground parts has been attributed to phenolic acids and flavonoids [13,19], essential oil components [20,21], and clerodane-type diterpene solidagoic acids [22].

High-performance thin-layer chromatography coupled with effect-directed analysis (HPTLC–EDA) is an efficient, rapid, and convenient tool for non-targeted screening of herb extracts for bioactive compounds without a time-consuming and costly isolation process [23,24]. The antibacterial profile of a sample can be determined by an HPTLC–direct bioautography (DB) method and the highly targeted characterization of compounds in the inhibition zones can be performed *in situ* on the adsorbent layer by various hyphenated techniques, such as mass spectrometry (HPTLC–MS). Thus, HPTLC hyphenations can promote the detection, separation, purification, isolation, and identification of antibacterial constituents of complex matrices [23,25]. The spectrum of microorganisms (or enzymes) is apt to be extended to exploit further the potential and the efficiency of the HPTLC–EDA in screening for promising chemicals suitable for treating different human, animal, and plant diseases. *Rhodococcus fascians* is a Gram-positive, aerobic phytopathogenic bacterium with a wide range of host plants, including strawberry, red beet, and tobacco [26]. This species is responsible for the leafy gall syndrome, an infectious plant disease that affects the plant appearance, triggering severe malformations in the inflorescence and the leaves because of the caused tissue hyperplasia [27]. Consequently, the development and the application of HPTLC–*R. fascians* assay is desirable.

The aim of this study was (1) the introduction of HPTLC–*R. fascians* bioassay, (2) the development of a HPTLC method that was required for non-targeted, effect-directed screening for antibacterial compounds present in the leaf extract of *S. gigantea*, (3) the characterization of the HPTLC zones of inhibition against Gram-positive (*Bacillus subtilis, B. subtilis* subsp. *spizizenii, R. fascians*) and Gram-negative (*Aliivibrio fischeri*) bacteria by HPTLC–MS, (4) the development of preparative flash chromatography, and semi-preparative HPLC methods for the bioassay-guided, semi-preparative fractionation and isolation of the active compounds, (5) the unambiguous structure elucidation of the isolated compounds by NMR measurements, and (6) the verification of the antibacterial activity of the isolates by both HPTLC–DB and *in vitro* microplate experiments.

2. Materials and methods

2.1. Materials

Glass- and aluminum-backed HPTLC and TLC silica gel 60 F_{254} layers (all 20 × 10 cm), methanol (LC-MS grade) and chloroform-*d* [99.8 atom% D, containing 0.03% (*V*/*V*) tetramethylsilane (TMS)] for NMR measurements were purchased from Merck (Darmstadt, Germany). Xprep preparative silica gel (pore size: 6.65 nm, particle size: 230–400 mesh) was supplied by LAB-EX (Budapest, Hungary). Solvents of analytical grade (acetone, chloroform (stabilized with amylene), ethyl acetate, methanol, dimethyl sulfoxide (DMSO), and *n*-hexane) and gradient grade acetonitrile were obtained from Reanal (Budapest, Hungary) or Molar Chemicals (Halásztelek, Hungary). Isopropyl acetate, gentamicin, and *p*-anisaldehyde were from Sigma-Aldrich (Budapest, Hungary). Bidistilled water by a Vitrotech VDB-3A apparatus (Vitro-Tech-Lab Ltd., Gyál, Hungary), while ultrapure water by a Millipore Direct-Q 3 UV Water Purification System (Merck) was prepared. Bromocresol green, glycerol, *D*-glucose, meat extract, potassium carbonate, potassium dihydrogen phosphate, disodium hydrogen phosphate, sodium chloride, and sodium hydroxide were bought from Reanal. Tryptone (from casein, pancreatic digest) was obtained from Reanal or Serva (Heidelberg, Germany), and agar was from Merck. Peptone (from meat, pancreatic digest) was supplied by Scharlau (Barcelona, Spain), yeast extract was from Scharlau or Microtrade (Budapest, Hungary), and sea salt mixture from Instant Ocean (Gambetta, France). 3-(4,5-Dimethylthiazol-2-yl)-2,5-diphenyltetrazolium bromide (MTT) was acquired from Carl Roth (Karlsruhe, Germany), concentrated sulfuric acid (96%) from Carlo Erba (Milan, Italy), and acetic acid from Lach-Ner (Neratovice, Czech Republic). Gram-positive, non-pathogenic *Bacillus subtilis* soil bacterium (strain F1276) was received by József Farkas, Central Food Research Institute, Budapest, Hungary, and *B. subtilis* subsp. *spizizenii* (DSM 618) was acquired from Merck. Gram-positive, plant pathogenic *Rhodococcus fascians* bacterium (strain NCAIM B.01608) was from the National Collection of Agricultural and Industrial Microorganisms, Budapest, Hungary. Gram-negative, naturally luminescent marine bacterium *Aliivibrio fischeri* (DSM 7151) was from Leibniz Institute, DSMZ, German Collection of Microorganisms and Cell Cultures, Berlin, Germany.

2.2. Sample origin and preparation

Leaves of *Solidago gigantea* Ait. were collected in July 2020 near Harta, in the Great Plain, Hungary (46° 41′ 51.5" N 19° 02′ 52.4" E, altitude: 90 m a. s. l.). A voucher herbarium specimen (accession number: HNHM-TRA 00027284) has been deposited in Hungarian Natural History Museum, Budapest, Hungary (Fig. S1). Leaf samples were dried at room temperature, protected from direct sunlight and finely milled by a coffee grinder (Sencor SCG 2050RD, Říčany, Czech Republic). The dried, ground samples (100 g) were consecutively macerated at room temperature with *n*-hexane (150 mg/mL, 3 × 72 h). The combined and filtered (Reanal filter paper, pore size: 7–10 µm) crude extract was concentrated under reduced pressure with a rotary evaporator (Rotavapor R-134, Büchi, Flawil, Switzerland) at 40 °C. This concentrated crude extract was employed for HPTLC analyses and isolation. Isolated compounds (**1–4**) were dissolved in chloroform or DMSO (2 mg/mL). Each sample was stored at +4 °C in the dark until analysis.

2.3. HPTLC–UV/FLD

Each sample was manually applied using a 10 µL microsyringe (Hamilton Company, Reno, NV, USA) as a 5 mm band with 10–20 mm track distance onto the HPTLC layer. The distance from the lower plate edge was 8 and 15 mm from the left side. After drying, HPTLC separation was performed in a pre-saturated (for 10 min) developing chamber (twin trough chamber, CAMAG, Muttenz, Switzerland) with chloroform – ethyl acetate – methanol 15:3:2, *V*/*V*/*V* (**MP1**) or *n*-hexane – isopropyl acetate – methanol – acetic acid 29:20:1:1, *V*/*V*/*V*/*V* (**MP2**) mobile phase up to a migration distance of 80 mm, which took approximately 20 min. The HPTLC chromatograms were dried in a cold stream of air using a hairdryer for 5 min and documented under a UV lamp (CAMAG) at 254 nm (UV) and 366 nm (FLD) using a digital camera (Cybershot DSC-HX60, Sony, Neu-Isenberg, Germany). HPTLC chromatograms developed with acidic **MP2** and intended for antibacterial assays were neutralized by pneumatic spraying (airbrush, Revell, Bünde, Germany) with a phosphate buffer solution (0.1 M, pH 7.5) [28]. Plates were cut (with a blade or smartCUT Plate Cutter, CAMAG) into smaller, identical pieces for various antibacterial assays or chemical derivatization. For the derivatization with *p*-anisaldehyde sulfuric acid reagent (anisaldehyde reagent) the layers were dipped into the mixture of 500 µL *p*-anisaldehyde, 10 mL acetic acid, 100 mL methanol, and 5 mL concentrated sulfuric acid (96%), heated at 110 C for 5 min (Advanced Hot Plate, VWR, Debrecen, Hungary), and documented at white light illumination in transmittance (Vis; 96891 Salobrena 2 LED lamp, Eglo Lux, Dunakeszi, Hungary) or reflectance mode. For the detection of acidic compounds, the layers were dipped into bromocresol green

reagent (10 mg bromocresol green, 25 mL ethanol, 0.1 M aqueous sodium hydroxide solution added until a dark blue color appeared), and after drying documented at white light illumination (Vis) in reflectance mode.

2.4. HPTLC-EDA

The preparation of *A. fischeri* [29] and *B. subtilis* (F1276) [30] bacterial suspensions, and the workflow of detecting an antibacterial effect were previously reported in detail. The procedure, developed for *B. subtilis* (F1276) was adapted to *B. subtilis* subsp. *spizizenii*. Briefly, the developed, neutralized and dried HPTLC chromatograms were manually dipped into the cell suspensions for 8 s. In cases of non-luminescent bacteria, this step was followed by a 2 h incubation at 37 °C (100% humidity, horizontal position in a polypropylene box lined with a wetted paper towel). The bioautograms were visualized with a vital dye staining using an aqueous MTT solution (1 mg/mL) and a further 0.5 h incubation at 37 °C (100% humidity). Bright zones against purplish background (caused by viable cells) indicated the presence of antibacterial compounds. In contrast, during the *A. fischeri* assays the reduced bioluminescence (the inhibitory effect) was immediately captured by a cooled CCD camera (iBright FL1500 Imaging System, Thermo Fisher Scientific, Budapest, Hungary) as dark spots on the bright background (grayscale image).

For the novel HPTLC–*R. fascians* antibacterial assay, culture suspension was prepared by growing the cells in Waksman's broth (5 g/L peptone, 5 g/L meat extract, 5 g/L sodium chloride, 10 g/L glucose, pH adjusted to 7.2 with a 40% aqueous sodium hydroxide solution) at 30 °C on an orbital shaker with a rotational speed of 130 rpm to reach the late log growth phase (OD_{600}, optical density at a wavelength of 600 nm = 1.4). The further procedure was identical to the general method described above for non-luminescent bacteria (optimal incubation temperature: 30 °C).

2.5. HPTLC-MS and FIA-MS

HPTLC–MS analyses were performed using a TLC–MS Interface 2 (with 4 × 2 mm oval elution head, CAMAG), and either (1) – a single quadrupole mass spectrometer (QMS; LCMS-2020, Shimadzu, Kyoto, Japan) with a binary solvent pump (LC-20AB, Shimadzu), or (2) – a dual-pressure linear ion trap mass spectrometer (LIT–MS^n; LTQ Velos mass, Thermo Fisher Scientific, Waltham, MA, USA) with a quaternary pump (Accela 1250 pump a part of the UHPLC system, Thermo Fisher Scientific). For flow injection analysis (FIA)–LIT-MS^n, samples were dissolved in acetonitrile and injected into MS with a constant flow rate of 25 µL/min (**1**, **3**), 10 µL/min (**2**), and 30 µL/min (**4**). LIT-MS^n was used for obtaining fragmentation patterns of desired compounds. Both MSs worked in electrospray ionization (ESI) mode. Prior to HPTLC–MS analyses, HPTLC plates were predeveloped with methanol – bidistilled water (4:1, *V*/*V*) up to a migration distance of 95 mm (twin trough chamber), followed by drying at 100 °C for 20 min (Advanced Hot Plate, VWR). Sample application and chromatographic development were performed as described in Section 2.3. Based on bioautograms the zones of interest were marked in parallel chromatograms with a soft pencil and eluted with methanol for approximately 45 s (HPTLC–ESI-QMS) or 60 s (HPTLC–ESI-LIT-MS^n) at a flow rate of 0.2 mL/min. Full scan ESI–MS spectra (scan range: *m*/*z* 200–950, scan speed: 790 amu/s) were recorded both in the negative and positive ionization mode for HPTLC–ESI-QMS and HPTLC–ESI-LIT-MS^n, and in the negative ionization mode for FIA–ESI-LIT-MS^n. The fragmentation pattern of the compounds was obtained at 45% collision energy and isolation width of *m*/*z* 1.0. The working parameters of ESI-QMS were as follows: nebulizer gas (N_2) flow rate 1.5 L/min, drying gas (N_2) flow rate 10 L/min, interface temperature 350 °C, heat block temperature 400 °C, desolvation line temperature 250 °C, detector voltage 1.1 kV in negative, 0.95 kV in positive ionization mode. The working parameters of ESI-LIT-MS^n were as follows: heat temperature 350 °C, capillary temperature 300 °C, sheath gas 30 a.u. (arbitrary units), auxiliary gas 10 a.u., spray voltage 3.00 kV [31], and S-lens RF level 69.0. A plate background (at the same hR_F) mass spectrum was subtracted from each analyte mass spectrum. Instrument operation and control, as well as data acquisition, processing, and evaluation, were carried out with LabSolutions 5.42v software (Shimadzu) for HPTLC–QMS and Xcalibur software (version 2.1.0; Thermo Fisher Scientific) for HPTLC–LIT-MS^n and FIA–LIT-MS^n.

2.6. Preparative fractionation and purification

The concentrated *n*-hexane leaf extract was first fractionated by preparative solid-phase extraction. The extract was dried onto the surface of the preparative silica gel (3 × 10 g) that was loaded above a manually packed silica gel stationary phase (80 × 25 mm). Fractionation was achieved by collecting eluates of about 10 mL with a stepwise gradient (acetone – chloroform 1:19, *V*/*V*, 80 mL; acetone – *n*-hexane 1:1, *V*/*V*, 90 mL; acetone, 80 mL). The solvent flow was accelerated by applying external pressure with an air compressor (HYD-24F, Hyundai, Seoul, South Korea). Fractions were investigated by HPTLC assays. Those with similar fingerprints and bioactivity were combined and dried under reduced pressure with a rotary evaporator at 40 °C.

The solid residue was suspended in *n*-hexane and submitted to an additional fractionation step. Normal-phase flash column chromatography separation was accomplished with a CombiFlash NextGen 300 (Teledyne Isco, Lincoln, NE, USA) chromatograph, utilizing a RediSep Rf Gold silica gel column (20–40 µm, 40 g, Teledyne Isco) as a stationary phase, and a flow rate of 30 mL/min with a gradient of *n*-hexane (A) and acetone (B): 0% B (0–0.5 min); 0–30% B (0.5–20.5 min); 30–50% B (20.5–25.5 min); 50–100% B (25.5–27.5 min). The chromatogram was recorded by continuous absorbance measurement at 205 and 215 nm.

Isolation of the selected compounds from the flash fractions was performed using an LCMS-2020 system (Shimadzu), including a binary gradient solvent pump (LC-20AB), a vacuum degasser, a thermostated autosampler, a column oven, a diode-array detector, and an electrospray ionization (ESI)-MS system, all controlled with LabSolutions 5.42v software (Shimadzu). An analytical RP-HPLC–DAD–ESI-MS method was developed and scaled up to a semi-preparative column. The analytical HPLC separation was achieved on a Luna pentafluorophenyl (PFP) column (250 × 4.6 mm i.d., 5 µm particle size, Phenomenex, Torrance, CA, USA) at 35 C at a flow rate of 0.7 mL/min with a gradient of 5% aqueous acetonitrile (A) and acetonitrile (B): 40–80% B (0–15 min); 80–95% B (15–25 min); 95–100% B (25–28 min); 100% B (28–35 min); 100–40% B (35–40 min). The injection volume was 3 µL. Chromatograms were monitored at 210 and 240 nm and TIC chromatograms were detected by MS with the following working parameters: nebulizer gas (N_2) flow rate 1.5 L/min, drying gas (N_2) flow rate 15 L/min, interface temperature 350 °C, heat block temperature 400 °C, desolvation line temperature 250 °C, detector voltage 4.5 kV. Full scan ESI-MS spectra (scan range: *m*/*z* 300–950, scan speed: 5000 amu/s) were recorded both in negative and positive ionization mode. Isolation was performed on a semi-preparative Luna PFP column (250 × 10 mm i.d., 5 µm particle size, Phenomenex) under the same conditions, but at a flow rate of 3.5 mL/min. The injection volume was 35 µL, and appropriate peaks were collected based on the chromatogram at 210 nm. The fractionation/purification protocol was repeated 70 times. The purity and bioactivity of combined fractions were surveyed by HPTLC assays. Bioactive eluates were

dried under reduced pressure with a rotary evaporator at 40 °C and transferred to NMR spectroscopy.

2.7. MIC and IC_{50} determination

Minimal inhibitory concentration (MIC) and half-maximal inhibitory concentration (IC_{50}) values of the isolated compounds (**1**–**4**) against Gram-positive *B. subtilis* subsp. *spizizenii* and *R. fascians* bacterial growth were determined by an *in vitro* broth microdilution method in 96-well non-treated flat-bottom microplate (VWR, catalog number: 734-2781) assays. Each sample (**1**–**4**) was dissolved in DMSO (2 mg/mL) and from an aliquot of 5 µL a two-fold dilution series (made in duplicate) was prepared in DMSO in a sterile box. Then 150 µL of bacterial suspension (10^5 CFU/mL) was added to each well and incubated by shaking at 900 rpm with a PHMP Twin Microplate Shaker-Incubator Thermoshaker (Grant Inc., Beaver Falls, PA, USA). The incubation temperature and time for *B. subtilis* subsp. *spizizenii* bacteria were 37 °C and 24 h, and for *R. fascians* bacterium 30 °C and 48 h, respectively. Gentamicin (0.1 mg/mL) was employed as a positive control, while DMSO was used as a negative control. OD_{600} values, indicating cell multiplication, were recorded by a Labsystems Multiscan MS 4.0 microplate reader spectrophotometer (Thermo Scientific, Waltham, MA, USA) immediately and after the incubation period (background was subtracted). Two parallel results were averaged and reported herein. Measured data were analyzed by GraphPad Prism 9 (version 9.2.0) software.

2.8. NMR spectroscopy

All NMR measurements were carried out on a Bruker Avance III HD 600 (600/151 MHz, 14.1 T) spectrometer equipped with a cryogenically cooled Prodigy BBO probe head at 295 K. Each isolated compound (**1**–**4**) was dissolved in 600 µL of deuterated chloroform [chloroform-*d*, 99.8 atom% D, containing 0.03% (*V*/*V*) tetramethylsilane (TMS)] and transferred to a standard 5 mm NMR tube for analysis. Instrument operation and control as well as data acquisition were accomplished with the Bruker TopSpin 3.5 software using standard pulse sequences available in their software library (Table S2–S5). Spectral data were processed and analyzed by MestReNova software (Mestrelab Research, Santiago de Compostela, Spain). ^{1}H and ^{13}C chemical shifts (δ) are reported in ppm, both referenced to the internal standard (TMS, $\delta_H = \delta_C = 0.00$ ppm), whereas spin-spin coupling constants (J) are provided in Hz. Structure elucidation and (complete) ^{1}H and ^{13}C resonance assignments were deduced from direct ^{1}H–^{13}C, long-range ^{1}H–^{13}C, ^{1}H–^{1}H scalar spin-spin connectivities, and ^{1}H–^{1}H dipolar couplings using conventional 1D (^{1}H, ^{13}C{^{1}H}) as well as homo- and heteronuclear 2D [^{1}H–^{1}H COSY, ^{1}H–^{13}C edHSQC ($^1J_{C-H} = 145$ Hz), ^{1}H–^{13}C HMBC ($^nJ_{C-H} = 8$ Hz), ^{1}H–^{1}H TOCSY (mixing time: 80 ms) and ^{1}H–^{1}H NOESY (mixing time: 300 ms)] experiments.

3. Results and discussion

3.1. Optimizing the extraction solvent and the HPTLC mobile phase

For the intended antibacterial profiling of giant goldenrod leaf, two different extraction solvents, ethanol, and *n*-hexane were tested, and the results were compared. The composition of the ethanol extract was more diverse. However, *n*-hexane was selected for the extraction, because it provided less matrix among the more polar compounds and interestingly could extract the non-polar and semi-polar bioactive compounds with higher efficiency than ethanol as evident in the *A. fischeri* and *B. subtilis* bioautograms (Fig. 1). Several HPTLC mobile phases without an acidic constituent were studied to reach a satisfactory separation of the zones of interest that were detectable at white light illumination after derivatization with the universal anisaldehyde reagent. Among the explored mobile phases, chloroform – ethyl acetate – methanol 15:3:2, *V*/*V*/*V* (**MP1**) led to an appropriate separation of the extracted compounds, hence it was used for further HPTLC analyses.

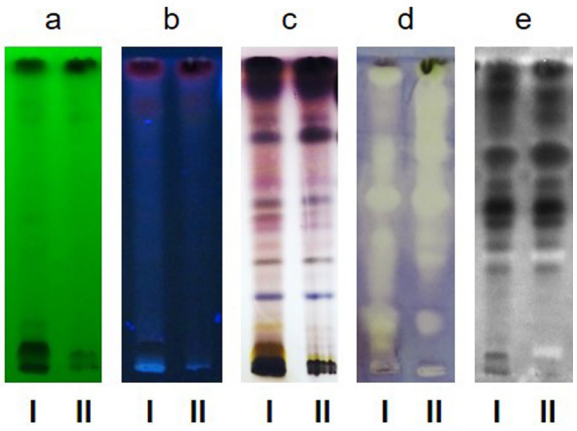

Fig. 1. HPTLC chromatograms (a–c) and bioautograms (d,e) of the *S. gigantea* ethanol (**I**) and *n*-hexane (**II**) leaf extract developed with chloroform – ethyl acetate – methanol 15:3:2 (*V*/*V*/*V*, **MP1**) and detected at 254 nm (a), 366 nm (b), after derivatization with anisaldehyde reagent at white light illumination (c), and after applying *B. subtilis* (d) and *A. fischeri* (e, grayscale image of the bioluminescence) antibacterial assays.

3.2. Sample pre-treatment monitored by HPTLC–EDA and HPTLC–MS

Due to the sample complexity, a two-step pre-cleaning method including a preparative solid-phase extraction (SPE) was followed by a normal-phase (NP) flash chromatography fractionation, which was applied before the large-scale isolation procedure.

The *n*-hexane extract of 100 g of dried leaves was purified by preparative SPE on a silica gel column in three parts yielding 21 (**SPE1**), 25 (**SPE2**), and 24 (**SPE3**) fractions, which were then investigated by HPTLC–Vis after derivatization with the anisaldehyde reagent (Fig. S2). Fractions 11 and 12 of each extraction (**SPE1**, **SPE2**, and **SPE3**) were combined and their bioactivity against *B. subtilis* was monitored by HPTLC–EDA. Based on the HPTLC–*B. subtilis* bioautogram, the targeted compounds responsible for the inhibition zones were present in the combined SPE fractions (Figs. 2 and S3). After purification, the active zone was observed as a distinct pinkish-purplish spot on the HPTLC–anisaldehyde chromatogram, which was characterized by HPTLC–ESI-QMS and HPTLC–ESI-LIT-MS^n. As for the HPTLC–ESI-QMS study (Fig. S3), mass signals were obtained in both ionization modes at *m*/*z* 347 $[M–H]^-$ and *m*/*z* 445 $[M–H]^-$ as well as at *m*/*z* 371 $[M+Na]^+$ and 469 $[M+Na]^+$, respectively, indicating the coelution of at least two compounds. HPTLC–ESI-LIT-MS^n measurements revealed the following MS fragmentation for the deprotonated molecule ($[M–H]^-$) at *m*/*z* 347 and at *m*/*z* 445, respectively: *m*/*z* 329, 303, 285, 267, 259, 257 (Fig. 2c) as well as *m*/*z* 345, 301, 283, 273, 257 (Fig. 2d,e).

The fractionation of the combined SPE fractions was carried out by NP flash chromatography providing 67 fractions (Fig. S4) that were examined by HPTLC–Vis after derivatization with anisaldehyde reagent (Fig. S5). Fractions having similar HPTLC fingerprints were combined and tested by HPTLC–antibacterial assays (Fig. 3) and HPTLC–MS (Fig. S6). HPTLC–MS studies revealed the presence of antibacterial compounds with identical mass signals as previously presented, in flash fractions 43–45 (denoted as **A**) and 46–

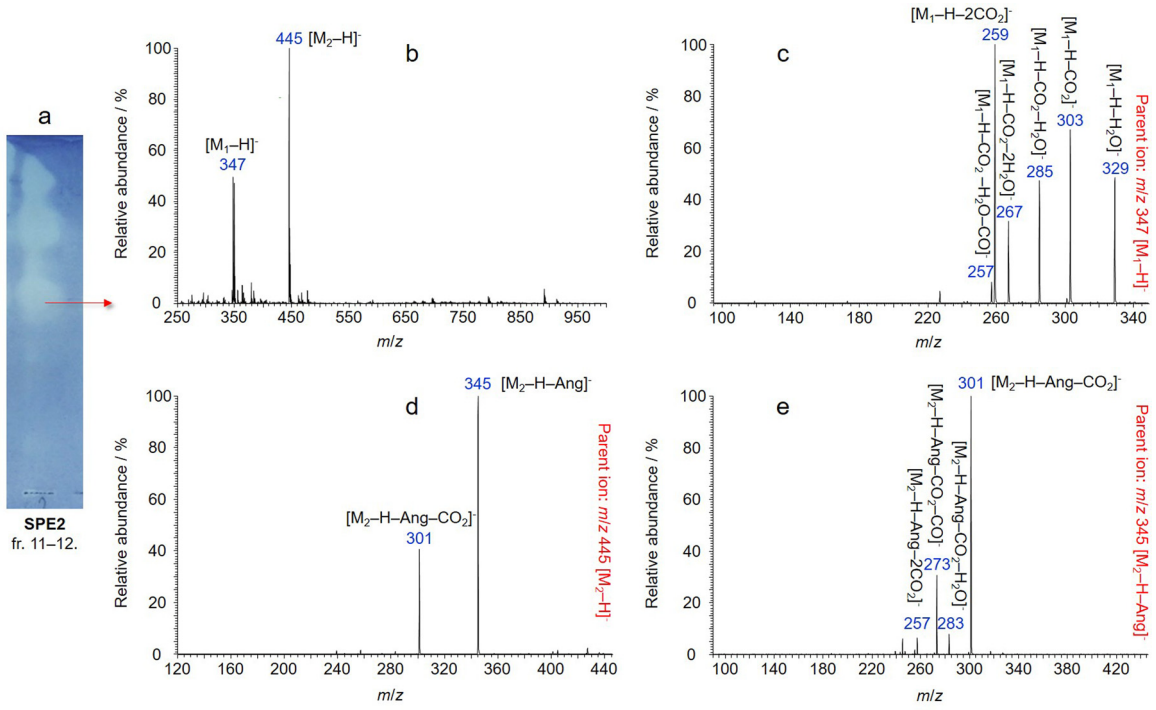

Fig. 2. HPTLC-*B. subtilis* bioautogram (a) of the combined **SPE2** fractions 11–12 developed with chloroform – ethyl acetate – methanol 15:3:2 (*V*/*V*/*V*, **MP1**) and HPTLC–ESI$^-$-LIT-MS^n spectra recorded from the zone of interest: full MS spectrum (b), MS/MS spectrum with the parent ion of *m*/*z* 347 [M–H]$^-$ (c), MS/MS spectrum with the parent ion of *m*/*z* 445 [M–H]$^-$ (d), MS^3 spectrum of the *m*/*z* 445 [M–H]$^-$ ion with the parent ion of *m*/*z* 345 [M–H–Ang]$^-$ (e), all of them labeled with the tentative assignment of the deprotonated molecules and the fragment ions. „Ang" abbreviation stands for angelic acid ($C_5H_8O_2$).

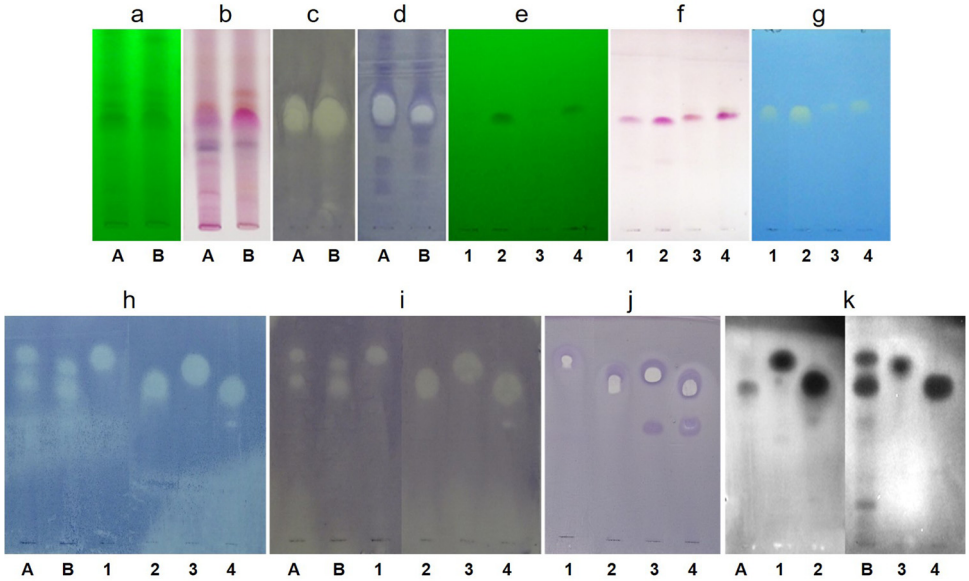

Fig. 3. HPTLC chromatograms and bioautograms of the flash fractions **A** and **B** as well as of the four isolated compounds (**1**–**4**) developed with chloroform – ethyl acetate – methanol 15:3:2 (*V*/*V*/*V*, **MP1**) (a–g), or *n*-hexane – isopropyl acetate – methanol – acetic acid 29:20:1:1 (*V*/*V*/*V*/*V*, **MP2**) (h–k). Detection was performed at 254 nm before derivatization (a and e) or at white light illumination after derivatization with anisaldehyde reagent (b and f) or bromocresol green staining (g) or after antibacterial assays with *B. subtilis* (c, i), *B. subtilis* subsp. *spizizenii* (h), *R. fascians* (d and j) and *A. fischeri* (k, grayscale image of the bioluminescence). Neutralization was used after development with acidic mobile phase (h–k).

48 (denoted as **B**), respectively (Fig. S6). Both fractions showed inhibition against *B. subtilis* and also in the novel HPTLC–*R. fascians* antibacterial assay and the acquired bright inhibition zones against the purple background at the same hR_F proved the antibacterial feature of the compounds with different molecular mass (Fig. 3a–d).

3.3. RP-HPLC isolation of the antibacterial compounds

The two combined flash chromatographic fractions **A** and **B** were subjected to RP-HPLC–DAD–ESI-MS analysis on a PFP column with an acetonitrile-water binary gradient system to separate the target compounds. During the HPLC method development, it was

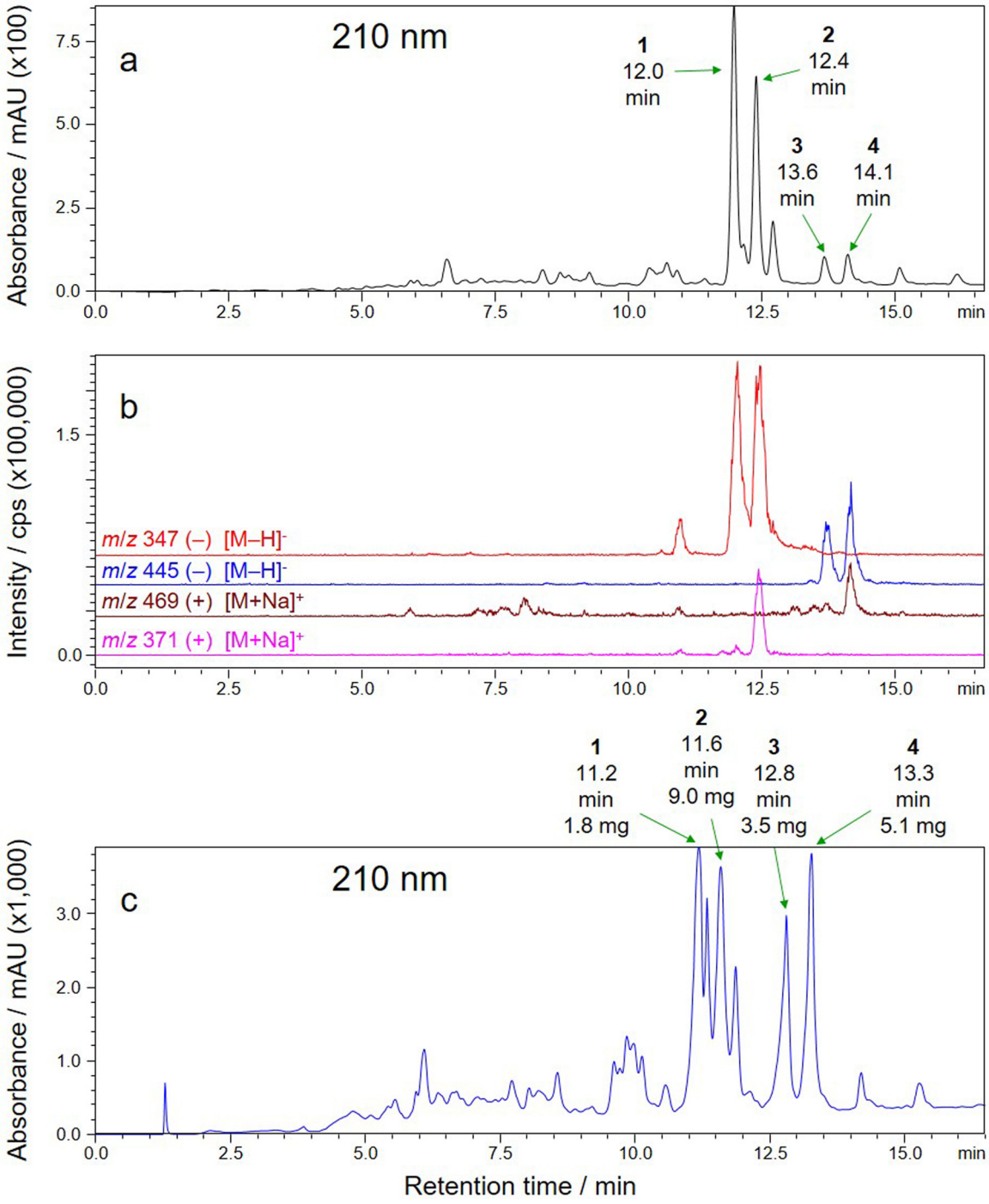

Fig. 4. UV (a) and extracted ion (b) chromatograms of the combined flash fraction obtained by analytical HPLC–DAD–ESI-MS analysis and UV chromatogram recorded by semi-preparative HPLC–DAD during the isolation of the four compounds (**1**–**4**) (c) labeling the retention times and the isolated amounts.

evident that both fractions surprisingly contained not only one but two constituents with the expected mass signals. It was doubtful whether they were structural isomers, therefore additional studies were required for clarification. Since these four compounds could be separated sufficiently in a single-run measurement, time and HPLC solvent could be saved by the use of the combination of the two fractions for the isolation. Thus, the separation of the four compounds from each other and also from the contaminants was achieved within 15 min with retention times of 12.0 min (**1**), 12.4 min (**2**), 13.6 min (**3**), and 14.1 min (**4**) illustrated on the chromatogram recorded at 210 nm (Fig. 4a). This is also evident on the EIC chromatograms (Fig. 4b) displaying the same deprotonated molecules and sodium adducts as previously detected: *m*/*z* 347 $[M–H]^-$ and *m*/*z* 371 $[M+Na]^+$ for **1** and **2**, as well as *m*/*z* 445 $[M–H]^-$ and 469 $[M+Na]^+$ for **3** and **4**, respectively.

With the scale-up of this analytical method, the semi-preparative purification and the isolation of the compounds 1–4 were performed on a PFP column (250 × 10 mm i.d.) by collecting fractions with the retention times of 11.2 min (**1**), 11.6 min (**2**), 12.8 min (**3**), and 13.3 min (**4**) (Fig. 4c). The quantity of the isolated compounds was sufficient to transfer them to NMR spectroscopy: 1.8 mg (**1**), 9.0 mg (**2**), 3.5 mg (**3**), and 5.1 mg (**4**).

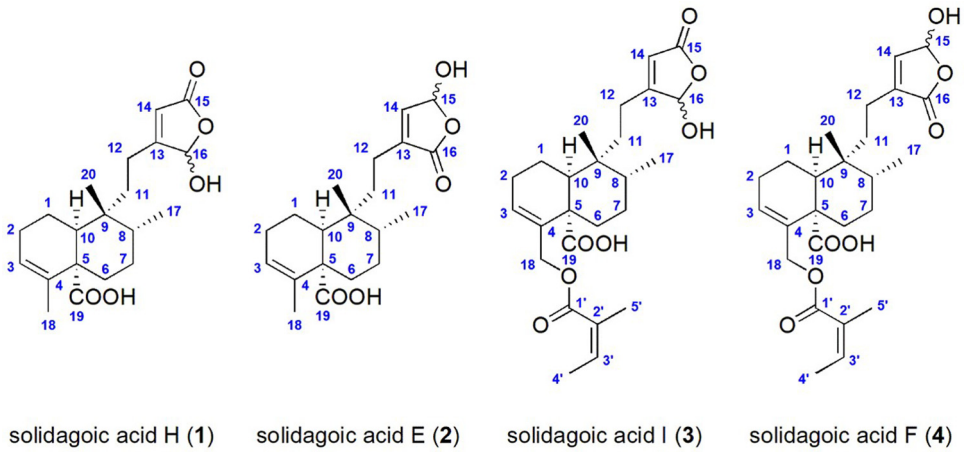

Fig. 5. Chemical structures and atom numbering (blue) of the four isolated clerodane diterpenoids.

3.4. The comprehensive characterization of isolated compounds

Isolates were analyzed by HPTLC–anisaldehyde and HPTLC–EDA using **MP1** and an acidic mobile phase, *n*-hexane – isopropyl acetate – methanol – acetic acid 29:20:1:1, *V*/*V*/*V*/*V* (**MP2**) to assess their purity and antibacterial activity (Fig. 3). In both flash fractions **A** and **B**, pinkish zones appeared at the same hR_F justifying that no undesired chemical transformations occurred. In addition, all isolates showed inhibition against the tested bacterial cells, also in the new HPTLC-*R. fascians* assay, at the identical hR_F reinforcing that the compounds visible after derivatization are responsible for the prominent antibacterial effect. Based on the chromatogram and the bioautogram, the purity of the samples seemed adequate. Considering the tailing peak and zone shape of the compounds **1**–**4** during the HPLC and HPTLC experiments, an acidic character was anticipated. Complementary HPTLC studies using acid-free **MP1** were carried out with bromocresol green stain providing a selective visualization of acids such as carboxylic acids. The appearance of bright yellow spots against a blue background at the hR_F of the isolated compounds supported the prediction (Fig. 3g). HPTLC–UV/FLD analyses unveiled weak absorbance at 254 nm and fluorescence at 366 nm of compounds **1**–**4**, explaining the necessity for derivatization. HPTLC–ESI-QMS (Fig. S7) and HPLC–DAD–ESI-QMS (Fig. S8) analyses of the isolated compounds confirmed that their purity (85–92%, calculated from HPLC–UV at 220 nm) was appropriate and they were not artifacts of the isolation procedure. However, the sodium and solvent adducts of the molecules and the dimers were observed with a higher signal intensity in the mass spectra compared to the former results.

The results of NMR measurements (Figs. S9–S79 and Table 1) enabled the unambiguous structure elucidation of the four isolated compounds identified as diterpenoids bearing *cis*-clerodane skeleton: solidagoic acid H (**1**), solidagoic acid E (**2**), solidagoic acid I (**3**), and solidagoic acid F (**4**) (Fig. 5). Each isolated compound contained a carboxyl group at C-19 that is considered as an atypical structural motif among the clerodanes [22]. The NMR resonance assignment was confirmed by comparing the reported spectral data [22]. The *trans* relative configuration between the methyl groups at C-17 and C-20 was also validated by their ^{13}C chemical shift difference ($\Delta\delta_{C\text{-}20\text{–}C\text{-}17}$) exceeding 10.0 ppm [32]. Solidagoic acid H, E, I, and F were isolated by Starks *et al.* [22] from the aerial parts of *S. virgaurea* (European goldenrod). However, to the best of our knowledge, the four *cis*-clerodane diterpenoids mentioned above have not yet been isolated from *S. gigantea*. Comparing Starks and colleagues' publication, a more complete NMR resonance assignment could be provided (Table 1). The missing chemical shifts for C-19 of solidagoic acid H, for C-16 of solidagoic acid E, for C-5 and C-19 of solidagoic acid I as well as for C-4, C-13, C-16, and C-1'–C-5' of solidagoic acid F could be determined, thus a complete ^1H and ^{13}C NMR resonance assignment was given for solidagoic acid E and F.

Clerodane diterpenes belong to the class of naturally occurring secondary metabolites possessing diverse biological and pharmacological activities (antibacterial, antifungal, antitumor, insect antifeedant, anti-inflammatory, antiulcer, antiplasmodial, and cytotoxic effect) [33]. In our recent study, eight antimicrobial clerodane diterpenes were isolated and characterized from the root of *S. gigantea* [10]. Two clerodane diterpenoids, 16α-hydroxy-cleroda-3,13(14)-*Z*-diene-15,16-olide and 16-oxo-cleroda-3,13(14)-*E*-diene-15-oic acid, isolated from the seeds of *Polyalthia longifolia* (Annonaceae), displayed a powerful antibacterial activity particularly against Gram-negative bacteria, including *Escherichia coli, Pseudomonas aeruginosa*, and *Salmonella typhimurium* with MIC values in the range of 0.78–1.56 µg/mL, so being a stronger antibiotic than gentamicin. They also efficiently inhibited the growth of Gram-positive bacteria, such as *B. subtilis* and *Clostridium sporogenes* with MIC values between 1.56 and 6.25 µg/mL, a comparable potency to that of gentamicin [34]. Two other clerodane diterpenes, 2-α-hydroxy-*cis*-cleroda-3,13(*Z*),8(17)-trien-15-oic acid and 2-α-acetoxy-*cis*-cleroda-3,13(Z),8(17)-trien-15-oic acid, isolated from the leaves and twigs of *Haplopappus foliosus* (Asteraceae), were highly active against five investigated Gram-positive bacteria (*Bacillus cereus, Bacillus coagulans, B. subtilis, Micrococcus luteus*, and *Staphylococcus aureus*) with MIC values in the range of 0.625–2.5 µg, slightly more potent than tetracycline, but they were inactive against five studied Gram-negative bacteria [35].

The four isolated compounds were also subjected to FIA–LIT-MS^n analysis to discover their mass spectrometric fragmentation pattern. A similar set of major fragment ions was produced from **1**–**2** and **3**–**4** upon collision-induced dissociation (CID) differing mainly in their abundance (Figs. S80–S83) and supporting the structural isomerism. MS^n spectra revealed the loss of small neutral fragments [44 Da (CO_2), 18 Da (H_2O), 28 Da (CO) for **1**–**4** and 100 Da ($C_5H_8O_2$, angelic acid) for only **3**–**4**] and appropriate combinations of these being formed via sequential losses proved by MS^3 and MS^4 spectra, which are in agreement with the structures proposed based on NMR experiments containing γ-hydroxybutenolide and carboxylic acid moiety. A distinct, significant peak at *m*/*z* 267 was observed in the MS/MS spectrum of **1** (Fig. S80b), being absent from that of **2** (Fig. S81), implying a unique double water loss took place. This propensity was confirmed by MS^4 analysis via the CID breakdown of the pre-

Table 1
^{1}H and ^{13}C NMR ($CDCl_3$, 600/151 MHz) resonance assignment of solidagoic acid H (1), E (2), I (3), and F (4).

	Solidagoic acid H (**1**)		Solidagoic acid E (**2**)		Solidagoic acid I (**3**)		Solidagoic acid F (**4**)	
#	^{1}H δ (ppm)	^{13}C δ (ppm)	^{1}H δ (ppm)	^{13}C δ (ppm)	^{1}H δ (ppm)	^{13}C δ (ppm)	^{1}H δ (ppm)	^{13}C δ (ppm)
1a	1.54 (ov., 1H)	19.3	1.53 (m, 1H)	19.4	1.58 (ov., 1H)	19.2	1.58 (ov., 1H)	19.3
1b	1.74 (m, 1H)		1.73 (m, 1H)		1.78 (m, 1H)		1.78 (m, 1H)	
2ab	2.10 (m, 2H)	26.2	2.09 (ov., 2H)	26.3	2.20 (m, 2H)	26.3	2.19 (m, 2H)	26.3
3	5.52 (br s, 1H)	123.7	5.51 (br s, 1H)	123.6	5.92 (ov., 1H)	128.4	5.92 (br s, 1H)	127.9
4		135.6		135.7		135.4		135.3
5		51.1		51.0		50.0		49.9
6a	1.45 (td, J = 13.5, 4.7 Hz, 1H)	29.0	1.42 (ov., 1H)	29.1	1.54 (ov., 1H)	29.8	1.53 (ov., 1H)	29.8
6b	2.33 (m, 1H)		2.32 (ov., 1H)		2.42 (m, 1H)		2.39 (ov., 1H)	
7a	1.38 (m, 1H)	27.8	1.35 (m, 1H)	27.8	1.40 (m, 1H)	27.8	1.36 (ov., 1H)	27.8
7b	1.68 (ov., 1H)		1.63 (ov., 1H)		1.67 (ov., 1H)		1.66 (ov., 1H)	
8	1.68 (ov., 1H)	36.7	1.66 (ov., 1H)	36.8	1.68 (ov., 1H)	36.5	1.66 (ov., 1H)	36.6
9		38.5		38.5		38.5		38.6
10	2.30 (m, 1H)	42.4	2.30 (ov., 1H)	42.3	2.35 (m, 1H)	42.3	2.37 (ov., 1H)	42.2
11a	1.53 (ov., 1H)	28.7	1.38 (ov., 1H)	28.8	1.55 (ov., 1H)	28.2 (br)	1.38 (ov., 1H)	28.7 (br)
11b	1.63 (ov., 1H)		1.61 (ov., 1H)		1.66 (ov., 1H)		1.65 (ov., 1H)	
12a	2.19 (br s, 1H)	22.2	2.09 (ov., 1H)	19.4	2.14 (ov., 1H)	22.1	2.12 (m, 1H)	19.6
12b	2.62 (br t, J = 13.9 Hz, 1H)		2.45 (br t, J = 14.1 Hz, 1H)		2.61 (br s, 1H)		2.45 (br t, J = 14.3 Hz, 1H)	
13		n. d.		138.9		n. d.		138.9
14	5.88 (s, 1H)	116.9	6.88 (br s, 1H)	143.6	5.89 (s, 1H)	116.5	6.88 (br s, 1H)	143.5
15		172.6	6.07 (s, 1H)	97.6		173.0	6.07 (ov., 1H)	97.5
16	5.96 (br s, 1H)	100.1		173.0	5.92 (ov., 1H)	100.6		172.9
17	0.86 (d, J = 6.3 Hz, 3H)	15.6	0.82 (d, J = 6.5 Hz, 3H)	15.7	0.84 (d, J = 5.6 Hz, 3H)	15.6	0.82 (d, J = 5.8 Hz, 3H)	15.6
18a	1.55 (s, 3H)	18.9	1.55 (s, 3H)	18.9	4.50 (s, 2H)	64.3	4.47 (d, J = 13.5 Hz, 1H)	64.4
18b							4.50 (d, J = 13.5 Hz, 1H)	
19		181.9		181.1		180.0		179.6
20	0.96 (s, 3H)	26.3	0.96 (s, 3H)	26.5	0.96 (s, 3H)	26.4	0.97 (s, 3H)	26.5
1'						167.7		167.8
2'						127.6		127.6
3'					6.05 (br q, J = 7.2 Hz, 1H)	138.5	6.07 (ov., 1H)	138.7
4'					1.97 (dq, J = 7.2, 1.6 Hz, 3H)	15.8	1.97 (dq, J = 7.3, 1.7 Hz, 3H)	15.8
5'					1.87 (br s, 3H)	20.6	1.89 (br s, 3H)	20.6

(ov.: overlapping peaks, n. d.: could not be determined)

cursor ion at m/z 285 [M–CO_2–H_2O] to yield a mass signal at m/z 267 [M–CO_2–2H_2O] (Fig. S80d), indicating the second water loss.

As all solidagoic acids exhibited a pronounced inhibition in HPTLC–*B. subtilis* subsp. *spizizenii* and HPTLC–*R. fascians* assays (Fig. 3) at the appropriate hR_F, confirming their antibacterial feature, their MIC and IC_{50} were investigated by microdilution assays against both strains (Table S1). Solidagoic acid I (**3**) displayed moderate antibacterial activity against *B. subtilis* subsp. *spizizenii* with a MIC of 64.5 µg/mL (IC_{50} was between 32.3 and 64.5 µg/mL). Similarly, solidagoic acid H (**1**) and I (**3**) exhibited a slight antibacterial effect against *R. fascians* with an IC_{50} of 43.5 µg/mL and 64.4 µg/mL, respectively. The MIC of solidagoic acid H was also determined as 64.5 µg/mL. Note that solidagoic acid E, F, and H (**1**, **2**, and **4**) against *B. subtilis* subsp. *spizizenii* as well as solidagoic acid E and F (**2** and **4**) did not reach the IC_{50} at the maximum concentration utilized. The antibacterial activity of these four compounds was investigated by Starks *et al.* [22] against *S. aureus* (strain 25923), IC_{50} values obtained by microdilution method were established as >64 µg/mL (**1**), >64 µg/mL (**2**), 37 µg/mL (**3**), not determined (**4**). Hence, solidagoic acid I (**3**) proved to be the most active compound out of the four isolates. The moderate antibacterial activity shown by these four *cis*-clerodane diterpenoids suggests that they can serve as a starting point for the synthesis of more potent compounds.

4. Conclusions

New analytical normal-phase HPTLC and preparative reversed-phase column chromatography methods were developed for the separation, effect-directed detection and isolation of closely related bioactive diterpene isomers. The combination of these methods enabled the discovery of antibacterial solidagoic acid E, F, H, and I, new in *S. gigantea*, which were identified by NMR. Complete ^{1}H and ^{13}C NMR resonance assignments of solidagoic acid E and F were given for the first time. Introducinga Gram-positive plant pathogenic bacterium into direct bioautography, a novel HPTLC–*R. fascians* bioassay was developed, in which the isolated solidagoic acids exhibited inhibition. Solidagoic acid H and I showed a moderate antibacterial effect against the Gram-positive *Bacillus subtilis* subsp. *spizizenii* and *R. fascians* also in microdilution assays, thus they can act as lead compounds in drug discovery. The orthogonal separations allowed by the consecutive use of normal- and reversed-phase stationary phases as well as complementary methods based on planar and column chromatography developed in this study can be used for the fishing of potential drug or pesticide candidates from complex matrices in general.

CRediT authorship contribution statement

Márton Baglyas: Methodology, Investigation, Formal analysis,

Writing original draft. **Péter G. Ott:** Bacteriological work, Writing review & editing. **Zsófia Garádi:** NMR investigation. **Vesna Glavnik:** Methodology, Investigation, Writing review & editing. **Szabolcs Béni:** NMR investigation. **Irena Vovk:** Methodology, Writing review & editing, Resources, Funding acquisition. **Ágnes M. Móricz:** Conceptualization, Supervision, Methodology, Resources, Writing review & editing, Funding acquisition.

Declaration of Competing Interest

The authors declare no competing financial interests.

Acknowledgments

This work was supported by the National Research, Development and Innovation Office of Hungary (NKFIH K128921), the Hungarian-Slovenian TÉT Grant (2019-2.1.11-TÉT-2020-00115) and the Slovenian Research Agency (ARRS; research core funding No. P1-0005 and the bilateral project BI-HU/21-22-007). Z. Garádi worked with the professional support of the Doctoral Student Scholarship Program of the Co-operative Doctoral Program of the Ministry of Innovation and Technology, financed by the National Research, Development and Innovation Fund (KDP-1007075).

Supplementary materials

Supplementary material associated with this article can be found, in the online version, at doi:10.1016/j.chroma.2022.463308.

References

[1] U. Maitra, C. Stephen, L.M. Ciesla, Drug discovery from natural products – Old problems and novel solutions for the treatment of neurodegenerative diseases, J. Pharm. Biomed. Anal. 210 (2022) 114553, doi:10.1016/j.jpba.2021.114553.
[2] N.E. Thomford, D.A. Senthebane, A. Rowe, D. Munro, P. Seele, A. Maroyi, K. Dzobo, Natural products for drug discovery in the 21st century: innovations for novel drug discovery, Int. J. Mol. Sci. 19 (2018) 1578–1606, doi:10.3390/ijms19061578.
[3] D.R. Schlaepfer, P.J. Edwards, R. Billeter, Why only tetraploid *Solidago gigantea* (Asteraceae) became invasive: a common garden comparison of ploidy levels, Oecologia 163 (2010) 661–673, doi:10.1007/s00442-010-1595-3.
[4] J. Leuschner, Anti-inflammatory, spasmolytic and diuretic effects of a commercially available *Solidago gigantea* Herb. extract, Arzneim. Forsch. 45 (1995) 165–168.
[5] D. Woźniak, S. Ślusarczyk, K. Domaradzki, A. Dryś, A. Matkowski, Comparison of polyphenol profile and antimutagenic and antioxidant activities in two species used as source of *Solidaginis herba* – goldenrod, Chem. Biodivers. 15 (2018) e1800023, doi:10.1002/cbdv.201800023.
[6] J. Zekič, I. Vovk, V. Glavnik, Extraction and analyses of flavonoids and phenolic acids from Canadian goldenrod and giant goldenrod, Forests 12 (2020) 40, doi:10.3390/f12010040.
[7] M. Marksa, K. Zymone, L. Ivanauskas, J. Radušienė, A. Pukalskas, L. Raudone, Antioxidant profiles of leaves and inflorescences of native, invasive and hybrid *Solidago* species, Ind. Crop. Prod. 145 (2020) 112123, doi:10.1016/j.indcrop.2020.112123.
[8] D. Kalemba, H. Marschall, P. Bradesi, Constituents of the essential oil of *Solidago gigantea* Ait, Flavour Fragr. J. 16 (2001) 19–26, doi:10.1002/1099-1026(200101/02)16:1)19::AID-FFJ940(3.0.CO;2-U.
[9] G. Benelli, R. Pavela, K. Cianfaglione, D.U. Nagy, A. Canale, F. Maggi, Evaluation of two invasive plant invaders in Europe (*Solidago canadensis* and *Solidago gigantea*) as possible sources of botanical insecticides, J. Pest Sci. 92 (2019) 805–821, doi:10.1007/s10340-018-1034-5.
[10] Á.M. Móricz, D. Krüzselyi, P.G. Ott, Z. Garádi, S. Béni, G.E. Morlock, J. Bakonyi, Bioactive clerodane diterpenes of giant goldenrod (*Solidago gigantea* Ait.) root extract, J. Chromatogr. A 1635 (2021) 461727, doi:10.1016/j.chroma.2020.461727.
[11] S.-H. Lee, H.-W. Oh, Y. Fang, S.-B. An, D.-S. Park, H.-H. Song, S.-R. Oh, S.-Y. Kim, S. Kim, N. Kim, A.S. Raikhel, Y.H. Je, S.W. Shin, Identification of plant compounds that disrupt the insect juvenile hormone receptor complex, Proc. Natl. Acad. Sci. U.S.A. 112 (2015) 1733–1738, doi:10.1073/pnas.1424386112.
[12] G. Reznicek, J. Jurenitsch, G. Michl, E. Haslinger, The first structurally confirmed saponin from *Solidago gigantea*: structure elucidation by modern NMR techniques, Tetrahedron Lett. 30 (1989) 4097–4100, doi:10.1016/S0040-4039(00)99331-6.
[13] B. Kołodziej, R. Kowalski, B. Kędzia, Antibacterial and antimutagenic activity of extracts aboveground parts of three *Solidago* species: *Solidago virgaurea* L., *Solidago canadensis* L. and *Solidago gigantea* Ait, J. Med. Plant Res. 5 (2011) 6770–6779, doi:10.5897/JMPR11.1098.
[14] S. Anžlovar, J.D. Koce, Antibacterial and antifungal activity of aqueous and organic extracts from indigenous and invasive species of goldenrod (*Solidago* spp.) grown in Slovenia, Phyton 54 (2014) 135–147, doi:10.12905/0380.phython54(1)2014-0135.
[15] A. Toiu, L. Vlase, D.C. Vodnar, A.-M. Gheldiu, I. Oniga, *Solidago graminifolia* L. Salisb. (Asteraceae) as a valuable source of bioactive polyphenols: HPLC profile, *in vitro* antioxidant and antimicrobial potential, Molecules 24 (2019) 2666–2680, doi:10.3390/molecules24142666.
[16] D. Krüzselyi, J. Bakonyi, P.G. Ott, A. Darcsi, P. Csontos, G.E. Morlock, Á.M. Móricz, Goldenrod root compounds active against crop pathogenic fungi, J. Agric. Food Chem. 69 (2021) 12686–12694, doi:10.1021/acs.jafc.1c03676.
[17] Á.M. Móricz, M. Jamshidi-Aidji, D. Krüzselyi, A. Darcsi, A. Böszörményi, P. Csontos, S. Béni, P.G. Ott, G.E. Morlock, Distinction and valorization of 30 root extracts of five goldenrod (*Solidago*) species, J. Chromatogr. A 1611 (2020) 460602, doi:10.1016/j.chroma.2019.460602.
[18] D. Mishra, S. Joshi, G. Bisht, S. Pilkhwal, Chemical composition and antimicrobial activity of *Solidago canadensis* Linn. root essential oil, J. Basic Clin. Pharm. 1 (2010) 187–190.
[19] C. Ferrante, A. Chiavaroli, P. Angelini, R. Venanzoni, G.A. Flores, L. Brunetti, M. Petrucci, M. Politi, L. Menghini, S. Leone, L. Recinella, G. Zengin, G. Ak, M.D. Mascio, F. Bacchin, G. Orlando, Phenolic content and antimicrobial and anti-inflammatory effects of *Solidago virga-aurea*, *Phyllanthus niruri*, *Epilobium angustifolium*, *Peumus boldus*, and *Ononis spinosa* extracts, Antibiotics 9 (2020) 783–803, doi:10.3390/antibiotics9110783.
[20] A.V. Tkachev, E.A. Korolyuk, W. Letchamo, Volatile oil-bearing flora of Siberia VIII: essential oil composition and antimicrobial activity of wild *Solidago virgaurea* L. from the Russian Altai, J. Essent. Oil Res. 18 (2006) 46–50, doi:10.1080/10412905.2006.9699382.
[21] H.S. Elshafie, D. Grul'ová, B. Baranová, L. Caputo, L.D. Martino, V. Sedlák, I. Camele, V.D. Feo, Antimicrobial activity and chemical composition of essential oil extracted from *Solidago canadensis* L. growing wild in Slovakia, Molecules 24 (2019) 1206–1217, doi:10.3390/molecules24071206.
[22] C.M. Starks, R.B. Williams, M.G. Goering, M. O'Neil-Johnson, V.L. Norman, J.-F. Hu, E. Garo, G.W. Hough, S.M. Rice, G.R. Eldridge, Antibacterial clerodane diterpenes from goldenrod (*Solidago virgaurea*), Phytochemistry 71 (2010) 104–109, doi:10.1016/j.phytochem.2009.09.032.
[23] Á.M. Móricz, P.G. Ott, T.T. Häbe, A. Darcsi, A. Böszörményi, Á. Alberti, D. Krüzselyi, P. Csontos, S. Béni, G.E. Morlock, Effect-directed discovery of bioactive compounds followed by highly targeted characterization, isolation and identification, exemplarily shown for *Solidago virgaurea*, Anal. Chem. 88 (2016) 8202–8209, doi:10.1021/acs.analchem.6b02007.
[24] G. Corni, V. Brighenti, F. Pellati, G.E. Morlock, Effect-directed analysis of bioactive compounds in *Cannabis sativa* L. by high-performance thin-layer chromatography, J. Chromatogr. A 1629 (2020) 461511, doi:10.1016/j.chroma.2020.461511.
[25] U. Jug, I. Vovk, V. Glavnik, D. Makuc, K. Naumoska, Off-line multidimensional high performance thin-layer chromatography for fractionation of Japanese knotweed rhizome bark extract and isolation of flavan-3-ols, proanthocyanidins and anthraquinones, J. Chromatogr. A 1637 (2021) 461802, doi:10.1016/j.chroma.2020.461802.
[26] M.L. Putnam, M.L. Miller, *Rhodococcus fascians* in herbaceous perennials, Plant Dis. 91 (2007) 1064–1076, doi:10.1094/PDIS-91-9-1064.
[27] E. Stes, I. Francis, I. Pertry, A. Dolzblasz, S. Depuydt, D. Vereecke, The leafy gall syndrome induced by *Rhodococcus fascians*, FEMS Microbiol. Lett. 342 (2013) 187–195, doi:10.1111/1574-6968.12119.
[28] Á.M. Móricz, D. Krüzselyi, V. Lapat, P.G. Ott, Acetylcholinesterase inhibitors in the giant goldenrod root, J. Chromatogr. B 1185 (2021) 123004, doi:10.1016/j.jchromb.2021.123004.
[29] Á.M. Móricz, T.T. Häbe, P.G. Ott, G.E. Morlock, Comparison of high-performance thin-layer with overpressured layer chromatography combined with direct bioautography and direct analysis in real time mass spectrometry for tansy root, J. Chromatogr. A 1603 (2019) 355–360, doi:10.1016/j.chroma.2019.03.068.
[30] Á.M. Móricz, T.T. Häbe, A. Böszörményi, P.G. Ott, G.E. Morlock, Tracking and identification of antibacterial components in the essential oil of *Tanacetum vulgare* L. by the combination of high-performance thin-layer chromatography with direct bioautography and mass spectrometry, J. Chromatogr. A 1422 (2015) 310–317, doi:10.1016/j.chroma.2015.10.010.
[31] L.-L. Xu, F.-X. Guo, S.-S. Chi, Z.-J. Wang, Y.-Y. Jiang, B. Liu, J.-Y. Zhang, Rapid screening and identification of diterpenoids in *Tinospora sinensis* based on high-performance liquid chromatography coupled with linear ion trap-orbitrap mass spectrometry, Molecules 22 (2017) 912–928, doi:10.3390/molecules22060912.
[32] Y. Nishidono, K. Tanaka, New clerodane diterpenoids from *Solidago altissima* and stereochemical elucidation via ^{13}C NMR chemical shift analysis, Tetrahedron 110 (2022) 132691, doi:10.1016/j.tet.2022.132691.
[33] R. Li, S.L. Morris-Natschke, K.-H. Lee, Clerodane diterpenes: sources, structures, and biological activities, Nat. Prod. Rep. 33 (2016) 1166–1226, doi:10.1039/C5NP00137D.
[34] M. Marthanda Murthy, M. Subramanyam, M. Hima Bindu, J. Annapurna, Antimicrobial activity of clerodane diterpenoids from *Polyalthia longifolia* seeds, Fitoterapia 76 (2005) 336–339, doi:10.1016/j.fitote.2005.02.005.
[35] A. Urzúa, R. Torres, L. Mendoza, F.D. Monache, Antibacterial new clerodane diterpenes from the surface of *Haplopappus foliosus*, Planta Med. 69 (2003) 675–677, doi:10.1055/s-2003-41118.